Displacement and equilibrium mesh-free formulation based on integrated radial basis functions for dual yield design

Phuc L.H. Ho [a,b] Canh V. Le [c,*] , T. Tran-Cong [d]

[a] *Faculty of Applied Mechanics and Civil Engineering, University of Technical Education - HCMC, Viet Nam*

[b] *Computational Engineering Laboratory, Institute for Computational Science and Technology, Ho Chi Minh City, Vietnam*

[c] *Department of Civil Engineering, International University - VNU HCM, Viet Nam*

[d] *Computational Engineering and Science Research Centre, University of Southern Queensland, Toowoomba, QLD 4350, Australia*

Abstract

This paper presents displacement and equilibrium mesh-free formulation based on integrated radial basis functions (iRBF) for upper and lower bound yield design problems. In these approaches, displacement and stress fields are approximated by the integrated radial basis functions, and the equilibrium equations and boundary conditions are imposed directly at the collocation points. In the paper it has been shown that direct nodal integration of the iRBF approximation can prevent volumetric locking in the kinematic formulation, and instability problems can also be avoided. Moreover, with the use of the collocation method in the static problem, equilibrium equations and yield conditions only need to be enforced at the nodes, leading to the reduction in computational cost. The mean value of the approximated upper and lower bound is found to be in excellent agreement with the available analytical solution, and can be considered as the actual collapse load multiplier for most practical engineering problems, for which exact solution is unknown.

Key words: Limit analysis; yield design; integrated radial basis function; mesh-free method; second order cone programming

* Corresponding author
Email address: lvcanh@hcmiu.edu.vn (Canh V. Le).

1 INTRODUCTION

The estimation of the plastic limit load of engineering structures has been of great interest to practical engineers. Elastic-plastic incremental analysis method can be employed to obtain such a limit load, but the plastic yield design (limit analysis) method has been viewed to be more effective [1,2], i.e. without performing a cumbersome series of incremental elastic-plastic analysis, and only requiring the knowledge of a local strength criterion. Based on bound theorems and numerical discretization techniques, the yield design approach can directly find the critical status of a structure or body under static loading and then the collapse load can be determined without intermediate steps.

A lower bound on the actual limit load of a structure or body can be achieved by using the static theorem and approximated stress fields, while the upper bound is obtained as a result of combining displacement-based model and kinematic theorem [11]. In the static yield design formulation, the assumed stress fields are often expressed in terms of nodal stress values. In the framework of equilibrium finite elements, these approximated fields are also required to satisfy a priori equilibrium conditions within elements and at their interfaces [3–6,11]. Due to these additional conditions, construction of such fields is often difficult. Compared with the equilibrium models, the displacement formulation is more popular. This may be because of the facts that the internal compatibility condition can be satisfied straightaway in the assembly scheme, and that essential (kinematic) boundary conditions can be enforced directly.

In recent decades, the development and application of mesh-free methods have attracted much attention due to their flexibility, e.g. requiring nodal data only and no need of nodal connectivity. The EFG method [7], one of the most widely used mesh-free methods, has been applied successfully to the framework of yield design problems [8–12], showing that the method is, in general, well suited for yield design problems and that accurate solutions can be obtained with a minimal computational cost. However, a typical limitation of the EFG method is that its shape functions do not hold Kronecker delta property, leading to difficulty in enforcing essential boundary conditions. Mesh-free methods using radial basis functions (RBFs) have also been developed in parallel [13–19]. These RBF-based methods have been applied successfully to a wide range of computational problems [20–26]. It has been shown that the RBF approximation is powerful to represent regular and smooth functions in arbitrary geometries and high-dimensional space, and enjoys spectral accuracy and exponential convergence [17].

The aim of this paper is to study the performance of the integrated radial basis function-based mesh-free method in the framework of yield design problems. The indirect/integrated radial basis function (iRBF) approaches pro-

posed in [28,29] are employed to approximate both displacement and stress fields. Multi-quadric iRBF method generally results in a high order approximation of the displacement fields (here, for convenience, 'displacement rate or velocity' is termed 'displacement'), and hence volumetric locking phenomena in the kinematic yield design formulation can be prevented. Moreover, the stress fields constructed based on iRBF are smooth over the entire problem domain, and consequently there is no need to enforce continuity conditions at interfaces within the problem domain. With the use of iRBF-approximated stress fields the strong-form of equilibrium equations can be satisfied in pointwise manner using collocation method. In addition, the iRBF-based approximation possesses the Kronecker delta property. As a result, kinematic and static boundary conditions can be imposed as easily as in the finite element method (FEM). Finally, the kinematic and static formulations based on iRBF discretization are formulated as a conic optimization problem, ensuring that they can be solved using available efficient solvers.

2 FUNDAMENTALS OF YIELD DESIGN THEORY

In this section, fundamentals of yield design theory are recalled, more details can be found in [45,51–54]. Consider a elastic-plastic body of area $\Omega \in \mathbb{R}^2$ with fixed boundary Γ_u and free portion Γ_t, satisfying $\Gamma_u \cup \Gamma_t = \Gamma$, $\Gamma_u \cap \Gamma_t = \oslash$, and is subjected to body forces $\mathbf{f}$ and surface tractions $\mathbf{t}$. Let Σ denotes a space of a statically admissible stress state, whereas $\mathscr{Y}$ is a space of a kinematically admissible displacement state. For smooth fields $\boldsymbol{\sigma}$ and $\mathbf{u}$, the classical form of the equilibrium equation can always be transformed to a more precise variational form as

$$a(\boldsymbol{\sigma}, \mathbf{u}) = F(\mathbf{u}), \quad \forall\, \mathbf{u} \in \mathscr{Y} \tag{1}$$

where the internal and external work rates can be respectively expressed as

$$a(\boldsymbol{\sigma}, \mathbf{u}) = \int_\Omega \boldsymbol{\sigma}^T \boldsymbol{\epsilon}(\mathbf{u})\, \mathrm{d}\Omega \tag{2}$$

$$F(\mathbf{u}) = \int_\Omega \mathbf{f}^T \mathbf{u}\, \mathrm{d}\Omega + \int_{\Gamma_t} \mathbf{t}^T \mathbf{u}\, \mathrm{d}\Gamma \tag{3}$$

where $\boldsymbol{\epsilon}(\mathbf{u}) = [\,\epsilon_{xx}\ \epsilon_{yy}\ \gamma_{xy}]^T$ are strain rates.

The static principle of yield design can now be expressed as

$$\lambda = \max\ \lambda^{-} \quad \text{s.t} \begin{cases} \lambda^{-} F(\mathbf{u}) = a(\boldsymbol{\sigma}, \mathbf{u}), \forall\, \mathbf{u} \in \mathscr{Y} \\ \exists\, \boldsymbol{\sigma} \in \mathscr{B}, \quad \mathscr{B} = \{\boldsymbol{\sigma} \in \Sigma \,|\, \psi(\boldsymbol{\sigma}(\mathbf{x})) \leq 0 \ \ \forall\, \mathbf{x} \in \Omega\} \end{cases} \tag{4}$$

where the so-called yield criterion $\psi(\boldsymbol{\sigma})$ is convex.

The kinematic principle of yield design, the dual form of (4), is

$$\lambda = \min_{\mathbf{u} \in \mathscr{C}}\ D(\mathbf{u}) \tag{5}$$

where the set $\mathscr{C}$ is defined by $\mathscr{C} = \{\mathbf{u} \in Y \,|\, F(\mathbf{u}) = 1\}$, and the plastic dissipation $D(\mathbf{u})$ is defined by

$$D(\mathbf{u}) = \max_{\boldsymbol{\sigma} \in \mathscr{B}}\ a(\boldsymbol{\sigma}, \mathbf{u}), \tag{6}$$

For the von Mises criterion, the power of dissipation can be formulated in terms of strain rates as

$$D(\boldsymbol{\epsilon}(\mathbf{u})) = \int_{\Omega} \sigma_p \sqrt{\boldsymbol{\epsilon}^T \boldsymbol{\Theta}\, \boldsymbol{\epsilon}} \tag{7}$$

where σ_p is the yield stress and

$$\boldsymbol{\Theta} = \begin{cases} \dfrac{1}{3} \begin{bmatrix} 4 & 2 & 0 \\ 2 & 4 & 0 \\ 0 & 0 & 1 \end{bmatrix} & \text{plane stress} \\ \begin{bmatrix} 1 & -1 & 0 \\ -1 & 1 & 0 \\ 0 & 0 & 1 \end{bmatrix} & \text{plane strain} \end{cases} \tag{8}$$

The incompressibility condition, i.e. $\boldsymbol{\Lambda}^T \boldsymbol{\epsilon} = 0$, where $\boldsymbol{\Lambda} = \begin{bmatrix} 1 & 1 & 0 \end{bmatrix}^T$, must be enforced for plane strain problem, ensuring that the plastic dissipation $D(\boldsymbol{\epsilon}(\mathbf{u}))$ is finite. This kinematic constraint results in a reduction of the number of degrees of freedom, and hence the volumetric locking problem occurs in the kinematic formulation using low-order approximation of displacement fields.

3 INDIRECT/INTEGRATED RADIAL BASIS FUNCTION (iRBF) METHOD

In this approach, usually the highest-order (second-order in the present case) derivative of the original approximate function is computed first. The first-order partial derivative and the original function are then constructed by successive integration as follows [29]

$$u^h_{,ij}(\mathbf{x}) = \sum_{I=1}^{\mathscr{N}} g_I(\mathbf{x})\, a_I = \mathbf{H}_2(\mathbf{x})\, \mathbf{b} \tag{9}$$

$$u^h_{,i}(\mathbf{x}) = \int \sum_{I=1}^{\mathscr{N}} g_I(\mathbf{x}) a_I \, dx_j = \sum_{I=1}^{\mathscr{N}+p_1} H_{1I}(\mathbf{x})\, a_I = \mathbf{H}_1(\mathbf{x})\, \mathbf{b} \tag{10}$$

$$u^h(\mathbf{x}) = \iint \sum_{I=1}^{\mathscr{N}} g_I(\mathbf{x}) a_I \, dx_j \, dx_i = \sum_{I=1}^{\mathscr{N}+p_2} H_{0I}(\mathbf{x})\, a_I = \mathbf{H}_0(\mathbf{x})\, \mathbf{b} \tag{11}$$

where $\mathscr{N}$ denotes the number of nodes in the local support domain, $\mathbf{b}$ is a vector consisting of the vector of coefficients and integration constants, and

$$\begin{aligned}
\mathbf{H}_2(\mathbf{x}) &= [\, g_1(\mathbf{x}),\, g_2(\mathbf{x}),\, \ldots, g_{\mathscr{N}}(\mathbf{x}),\, \underbrace{0,\, \ldots, 0}_{p2}] \\
\mathbf{H}_1(\mathbf{x}) &= [\, H_{11}(\mathbf{x}),\, H_{12}(\mathbf{x}),\, \ldots, H_{1\mathscr{N}+p1}(\mathbf{x}),\, \underbrace{0,\, \ldots, 0}_{p1}] \qquad (12) \\
\mathbf{H}_0(\mathbf{x}) &= [\, H_{01}(\mathbf{x}),\, H_{02}(\mathbf{x}),\, \ldots, H_{0\mathscr{N}+p2}(\mathbf{x})] \qquad (13)
\end{aligned}$$

in which p_1 and p_2 are the number of integration constants, and $p_2 = 2p_1$; detailed calculation of $H_{1I}(\mathbf{x})$ and $H_{0I}(\mathbf{x})$ can be found in [28,29]. In this study, multi-quadrics (MQ) basis function, which is ranked the best in terms of accuracy among RBFs [13,28], will be employed. MQs are defined by

$$g_I(\mathbf{x}) = \sqrt{r_I^2 + c_I^2} \tag{14}$$

where $r_I = \|\mathbf{x} - \mathbf{x}_I\|$, the shape parameter $c_I = \beta\, d_I$ (β is a positive scalar), and d_I is the minimum of distances from node I to its neighbors in the support domain.

The evaluation of Equation (11) at a set of collocation points yields the following equation in matrix form

$$\mathbf{u} = \mathbf{H}_Q\, \mathbf{b} \tag{15}$$

where

$$\mathbf{H}_Q = \begin{bmatrix} \dots & \dots & \dots & \dots \\ H_{01}(\mathbf{x}_k) & H_{02}(\mathbf{x}_k) & \dots & H_{0\mathscr{N}+p_2}(\mathbf{x}_k) \\ \dots & \dots & \dots & \dots \end{bmatrix} \tag{16}$$

By inversion, the vector $\mathbf{b}$ is expressed in terms of nodal function values $\mathbf{u}$ as

$$\mathbf{b} = \mathbf{H}_Q^{-1}\,\mathbf{u} \tag{17}$$

Substituting $\mathbf{b}$ into Equations (9) – (11), we obtain

$$u^h(\mathbf{x}) = \mathbf{H}_0(\mathbf{x})\,\mathbf{H}_Q^{-1}\,\mathbf{u} = \mathbf{\Phi}\,\mathbf{u} \tag{18}$$

$$u^h_{,i}(\mathbf{x}) = \mathbf{H}_1(\mathbf{x})\,\mathbf{H}_Q^{-1}\,\mathbf{u} = \mathbf{\Phi}_{,i}\,\mathbf{u} \tag{19}$$

$$u^h_{,ij}(\mathbf{x}) = \mathbf{H}_2(\mathbf{x})\,\mathbf{H}_Q^{-1}\,\mathbf{u} = \mathbf{\Phi}_{,ij}\,\mathbf{u} \tag{20}$$

in which the shape functions and its derivatives are defined by

$$\begin{aligned} \Phi_k(\mathbf{x}) &= \sum_{I=1}^{\mathscr{N}} H_{0I}(\mathbf{x})\widehat{\chi}_{Ik} \\ \Phi_{k,i}(\mathbf{x}) &= \sum_{I=1}^{\mathscr{N}} H_{1I}(\mathbf{x})\widehat{\chi}_{Ik} \\ \Phi_{k,ij}(\mathbf{x}) &= \sum_{I=1}^{\mathscr{N}} g_I(\mathbf{x})\widehat{\chi}_{Ik} \end{aligned} \tag{21}$$

where $\widehat{\chi}_{Ik}$ is the (I,k) element of the matrix $\mathbf{H}_Q^{-1}$.

It should be noted that the iRBF shape functions satisfy the Kronecker-delta property, and hence boundary conditions can be enforced in a way similar to one in the finite element method.

4 DUAL YIELD DESIGN FORMULATION USING THE iRBF METHOD

4.1 iRBF discretization of kinematic formulation

In a numerical upper-bound yield design problem, the displacement fields of the problem domain can be approximated by discretization methods. The approximate displacement fields can be expressed in terms of nodal displacement

values as

$$\mathbf{u}^h(\mathbf{x}) = \begin{bmatrix} u \\ v \end{bmatrix} = \sum_{I=1}^{\mathscr{N}} \Phi_I(\mathbf{x}) \begin{bmatrix} u_I \\ v_I \end{bmatrix} \tag{22}$$

where $\Phi_I(\mathbf{x})$ are the iRBF shape functions described above.

The strain rates are then calculated by

$$\boldsymbol{\epsilon}(\mathbf{x}) = \begin{bmatrix} \epsilon_{xx} \\ \epsilon_{yy} \\ \gamma_{xy} \end{bmatrix} = \sum_{I=1}^{\mathscr{N}} \begin{bmatrix} \Phi_{I,x}(\mathbf{x}) & 0 \\ 0 & \Phi_{I,y}(\mathbf{x}) \\ \Phi_{I,y}(\mathbf{x}) & \Phi_{I,x}(\mathbf{x}) \end{bmatrix} \begin{bmatrix} u_I \\ v_I \end{bmatrix} = \mathbf{B}(\mathbf{x})\,\mathbf{d} \tag{23}$$

where $\mathbf{d}$ is the nodal displacement vector and $\mathbf{B}$ is the so-called strain-displacement matrix, and they are given by

$$\mathbf{d}^T = [u_1, u_2, \ldots, u_{\mathscr{N}}, v_1, v_2, \ldots, v_{\mathscr{N}}] \tag{24}$$

$$\mathbf{B} = \begin{bmatrix} \mathbf{B}_{xx} \\ \mathbf{B}_{yy} \\ \mathbf{B}_{xy} \end{bmatrix} = \begin{bmatrix} \Phi_{1,x} & \Phi_{2,x} & \ldots & \Phi_{\mathscr{N},x} & 0 & 0 & \ldots & 0 \\ 0 & 0 & \ldots & 0 & \Phi_{1,y} & \Phi_{2,y} & \ldots & \Phi_{\mathscr{N},y} \\ \Phi_{1,y} & \Phi_{2,y} & \ldots & \Phi_{\mathscr{N},y} & \Phi_{1,x} & \Phi_{2,x} & \ldots & \Phi_{\mathscr{N},x} \end{bmatrix} \tag{25}$$

The internal dissipation power is computed as

$$D = \int_{\Omega} \sigma_0 \sqrt{\boldsymbol{\epsilon}^T \boldsymbol{\Theta}\, \boldsymbol{\epsilon}}\; d\Omega = \sum_{I=1}^{\mathscr{N}} \sigma_0 A_I \sqrt{(\mathbf{B}_I\,\mathbf{d})^T \boldsymbol{\Theta}\, \mathbf{B}_I\,\mathbf{d}} \tag{26}$$

where A_I is the area of the I^{th} nodal representative domain, i.e. Voronoi cell.

In fact, a form containing a sum of norms can be used to compute the power of internal dissipation as the following expression

$$D = \sum_{I=1}^{\mathscr{N}} \sigma_0 A_I \|\boldsymbol{\rho}_I\| \tag{27}$$

where $\boldsymbol{\rho}_I$ are additional variables defined by

$$\boldsymbol{\rho}_I = \begin{cases} \begin{bmatrix} \rho_1 \\ \rho_2 \\ \rho_3 \end{bmatrix} = \dfrac{1}{\sqrt{3}} \begin{bmatrix} 2 & 0 & 0 \\ 1 & \sqrt{3} & 0 \\ 0 & 0 & 1 \end{bmatrix} \mathbf{B}_I \mathbf{d} & \text{plane stress} \\ \\ \begin{bmatrix} \rho_1 \\ \rho_2 \end{bmatrix} = \begin{bmatrix} \mathbf{B}_{xxI}\mathbf{d} - \mathbf{B}_{yyI}\mathbf{d} \\ 2\mathbf{B}_{xyI}\mathbf{d} \end{bmatrix} & \text{plane strain} \end{cases} \tag{28}$$

Hence, the optimization problem (5) associated with the iRBF method can now be rewritten as

$$\begin{aligned} \lambda^+ = \min & \sum_{I=1}^{\mathscr{N}} \sigma_0 A_I \|\boldsymbol{\rho}_I\| \\ \text{s.t} & \begin{cases} \mathbf{d} = \mathbf{0} & \text{on } \Gamma_u \\ F(\mathbf{d}) = 1 \end{cases} \end{aligned} \tag{29}$$

Introducing auxiliary variables $t_1,\ t_2,\ \ldots,\ t_{\mathscr{N}}$, the problem (29) can be formulated in the form of a standard conic programming as

$$\begin{aligned} \lambda^+ = \min & \sum_{I=1}^{\mathscr{N}} \sigma_0 A_I t_I \\ \text{s.t} & \begin{cases} \mathbf{d} = \mathbf{0} & \text{on } \Gamma_u \\ F(\mathbf{d}) = 1 \\ ||\boldsymbol{\rho}_I|| \leq t_I \ \ I = 1, 2, \ldots, \mathscr{N} \end{cases} \end{aligned} \tag{30}$$

Note that for plane strain problems, incompressibility conditions, $\boldsymbol{\Lambda}^T \boldsymbol{\epsilon} = 0$, must be introduced. If low-order displacement approximations are used, volumetric locking phenomena in the kinematic formulations associated with the von Mises may occur due to these incompressibility conditions. However, here the iRBF method results in high-order displacement fields, and hence volumetric locking problem can be prevented. Moreover, it is evident that the size of optimization problem (30) depends on the number of integration points to be used. In this paper, nodal integration technique is used, and hence the size of the resulting optimization problem is kept to be minimum.

While in the upper bound formulation the displacement fields are approximated, here the stress fields need to be approximated. With the use of the iRBF method, approximations of these stress fields can be presented as

$$\boldsymbol{\sigma}^h(\mathbf{x}) = \begin{bmatrix} \sigma^h_{xx} \\ \sigma^h_{yy} \\ \sigma^h_{xy} \end{bmatrix} = \sum_{I=1}^{\mathscr{N}} \Phi_I(\mathbf{x}) \begin{bmatrix} \sigma_{xxI} \\ \sigma_{yyI} \\ \sigma_{xyI} \end{bmatrix} = \mathbf{C}\,\mathbf{s} \tag{31}$$

where

$$\mathbf{s}^T = [\sigma_{xx1}, \sigma_{xx2}, \ldots, \sigma_{xx\mathscr{N}}, \sigma_{yy1}, \sigma_{yy2}, \ldots, \sigma_{yy\mathscr{N}}, \sigma_{xy1}, \sigma_{xy2}, \ldots, \sigma_{xy\mathscr{N}}] \tag{32}$$

$$\mathbf{C} = \begin{bmatrix} \mathbf{C}_{xx} \\ \mathbf{C}_{yy} \\ \mathbf{C}_{xy} \end{bmatrix} = \begin{bmatrix} \Phi_1 & \Phi_2 & \ldots & \Phi_{\mathscr{N}} & 0 & 0 & \ldots & 0 & 0 & 0 & \ldots & 0 \\ 0 & 0 & \ldots & 0 & \Phi_1 & \Phi_2 & \ldots & \Phi_{\mathscr{N}} & 0 & 0 & \ldots & 0 \\ 0 & 0 & \ldots & 0 & 0 & 0 & \ldots & 0 & \Phi_1 & \Phi_2 & \ldots & \Phi_{\mathscr{N}} \end{bmatrix} \tag{33}$$

These approximated stress fields must be ensured to be statically admissible, meaning that equilibrium and continuity conditions within elements and on their boundary must be satisfied. While the strong form of equilibrium equations can be treated using collocation method, its equivalent weak form (involving integrals) is often handled using the weighted residual method. The strong-form method is simple and fast, and hence the collocation method using the iRBF will be considered in this study. The equilibrium equations can be imposed at $\mathscr{N}$ nodes, and are expressed as

$$\mathbf{A}_1\boldsymbol{\sigma}_1 + \mathbf{A}_2\boldsymbol{\sigma}_3 = \mathbf{0} \tag{34}$$

$$\mathbf{A}_1\boldsymbol{\sigma}_3 + \mathbf{A}_2\boldsymbol{\sigma}_2 = \mathbf{0} \tag{35}$$

where

$$\mathbf{A}_1 = \begin{bmatrix} \ldots & \ldots & \ldots & \ldots \\ \Phi_{1,x}(\mathbf{x}_k) & \Phi_{2,x}(\mathbf{x}_k) & \ldots & \Phi_{\mathscr{N},x}(\mathbf{x}_k) \\ \ldots & \ldots & \ldots & \ldots \end{bmatrix}_{\mathscr{N}\times\mathscr{N}} \tag{36}$$

$$\mathbf{A}_2 = \begin{bmatrix} \dots & \dots & \dots & \dots \\ \Phi_{1,y}(\mathbf{x}_k) & \Phi_{2,y}(\mathbf{x}_k) & \dots & \Phi_{\mathscr{N},y}(\mathbf{x}_k) \\ \dots & \dots & \dots & \dots \end{bmatrix}_{\mathscr{N}\times\mathscr{N}} \tag{37}$$

$$\boldsymbol{\sigma}_1 = \begin{bmatrix} \sigma_{xx1} & \dots & \sigma_{xx\mathscr{N}} \end{bmatrix}^T \tag{38}$$

$$\boldsymbol{\sigma}_2 = \begin{bmatrix} \sigma_{yy1} & \dots & \sigma_{yy\mathscr{N}} \end{bmatrix}^T \tag{39}$$

$$\boldsymbol{\sigma}_3 = \begin{bmatrix} \sigma_{xy1} & \dots & \sigma_{xy\mathscr{N}} \end{bmatrix}^T \tag{40}$$

Additionally, the approximated stress fields must belong to a convex domain, $\mathscr{B}$. In other words, these stress fields must satisfy the following second-order cone constraints obtaining from the von Mises criterion

$$\boldsymbol{\sigma}^h(\mathbf{x}) \in \mathscr{B} \equiv \begin{cases} \mathscr{L}_{PS} = \left\{ \boldsymbol{\rho} \in R^3 \;\middle|\; \rho_1 \geq \|\rho_{2\to 4}\|_{L^2} = \sqrt{\rho_2^2 + \rho_3^2 + \rho_4^2} \right\} & \text{plane stress} \\ \mathscr{L}_{PD} = \left\{ \boldsymbol{\rho} \in R^3 \;\middle|\; \rho_1 \geq \|\rho_{2\to 3}\|_{L^2} = \sqrt{\rho_2^2 + \rho_3^2} \right\} & \text{plane strain} \end{cases} \tag{41}$$

where

$$\rho_1 = \sigma_0 \tag{42}$$

$$\boldsymbol{\rho}_{2\to 4} = \begin{bmatrix} \rho_2 \\ \rho_3 \\ \rho_4 \end{bmatrix} = \frac{1}{2} \begin{bmatrix} 2 & -1 & 0 \\ 0 & \sqrt{3} & 0 \\ 0 & 0 & 2\sqrt{3} \end{bmatrix} \mathbf{C}\,\mathbf{s} \quad \text{plane stress} \tag{43}$$

$$\boldsymbol{\rho}_{2\to 3} = \begin{bmatrix} \rho_2 \\ \rho_3 \end{bmatrix} = \begin{bmatrix} \frac{1}{2}(\mathbf{C}_{xx}\mathbf{s} - \mathbf{C}_{yy}\mathbf{s}) \\ \mathbf{C}_{xy}\mathbf{s} \end{bmatrix} \quad \text{plane strain} \tag{44}$$

Hence the static yield design formulation (4) can now be expressed as

$$\lambda^- = \max\ \lambda$$
$$\text{s.t} \begin{cases} \mathbf{A}_1\boldsymbol{\sigma}_1 + \mathbf{A}_2\boldsymbol{\sigma}_3 = \mathbf{0} \\ \mathbf{A}_1\boldsymbol{\sigma}_3 + \mathbf{A}_2\boldsymbol{\sigma}_2 = \mathbf{0} \\ \boldsymbol{\rho}^k \in \mathscr{L}^k,\ k = 1,\ 2,\ \ldots,\ \mathscr{N} \end{cases} \tag{45}$$

and accompanied by appropriate boundary conditions.

It should be emphasized that in the present static formulation equilibrium equations and yield criterion are enforced at nodes only, and therefore the strict property of the lower bound λ^- is not guaranteed. However, using a fine nodal distribution one can hope to achieve a reliable approximated lower bound on the actual limit load multiplier. Moreover, by enforcing the equilibrium equations and yield criterion at nodes only the number of constraints in optimization problem (45) is kept to be minimum, and hence the presented static method is computationally inexpensive.

5 NUMERICAL EXAMPLES

The described procedures are tested by their application to solve various problems for which, in most cases, exact and numerical solutions are available. Upper and lower bound solutions based on direct radial basis function (dRBF) are also carried out for comparison purpose. Optimization problems (30) and (45) are implemented in the Matlab environment. Mosek optimization solver version 6.0 is used to solve the conic optimization problem obtained (using a 2.8 GHz Intel Core i5 PC running Window 7).

5.1 Prandtl problem

The first example is the classical punch problem presented in [30], as shown in Figure 1. Due to symmetry, a rectangular region of dimensions $B = 5$ and $H = 2$ is considered. Appropriate displacement and stress boundary conditions are enforced as shown in Figure 2. For a load of $2\tau_0$, the analytical limit multiplier is $\lambda = 2 + \pi = 5.142$.

Approximations of upper and lower bounds on the actual limit load for both dRBF and iRBF methods with various nodal discretizations are reported in Table 1. From these results, it can be seen that for both kinematic and static formulations the iRBF-based method can provide more accurate solutions than the dRBF-based method. Convergence analysis and relative errors in collapse multipliers versus number of variables are also shown in Figures 3 and 4,

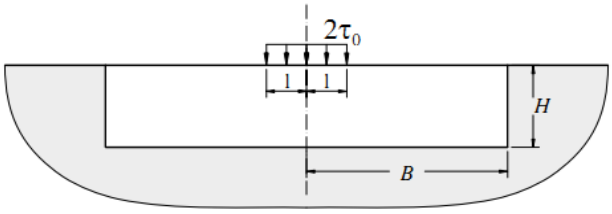

Fig. 1. Prandtl problem: geometry and loading

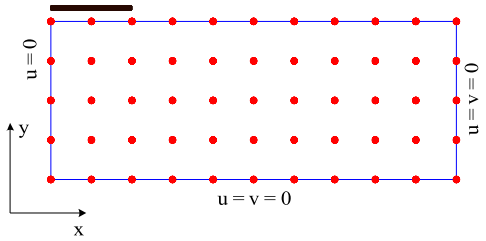

(a) Displacement boundary conditions

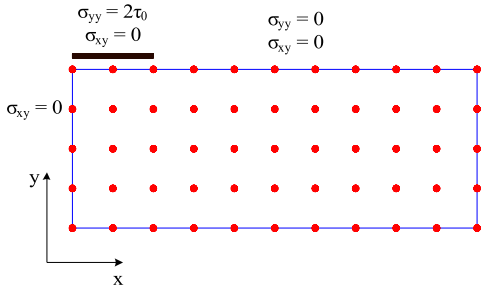

(b) Stress boundary conditions

Fig. 2. Prandtl problem: appropriate displacement and stress boundary conditions

respectively. It should be stressed that the mean values of upper and lower approximations obtained using the iRBF-based numerical procedures are in excellent agreement with the analytical solutions for all nodal discretizations, as shown in Figure 3, with less than 0.4% even for coarse nodal distribution. Furthermore, as mentioned, the present procedure can not theoretically provide strict lower bound solutions, it is evident that all approximated lower bound results are below the exact value.

Note that in the kinematic formulation, volumetric (or isochoric) locking often occurs when adding the incompressibility condition to the low-order displacement based yield design problem. The volumetric locking behavior of the Prandtl yield design problem has been studied in [35,12]. In these papers, it has been demonstrated that when smoothed strains were used, the volumetric locking problem can be eliminated. Here, we have shown that the iRBF method used in combination with direct nodal integration can remove such the volumetric locking behavior and also result in stable and accurate solutions.

Table 1
Prandtl problem: upper and lower bound approximation of collapse multiplier

Nodes	dRBF				iRBF			
	Upper-bound		Lower-bound		Upper-bound		Lower-bound	
	λ^+	e (%)	λ^-	e (%)	λ^+	e (%)	λ^-	e (%)
40	6.857	33.35	2.761	46.31	6.036	17.39	4.218	17.97
160	5.548	7.90	4.244	17.46	5.279	2.66	4.960	3.54
360	5.289	2.86	4.800	6.65	5.209	1.30	5.061	1.58
640	5.211	1.34	5.042	1.95	5.191	0.95	5.108	0.66
1000	5.189	0.91	5.125	0.33	5.180	0.74	5.134	0.16

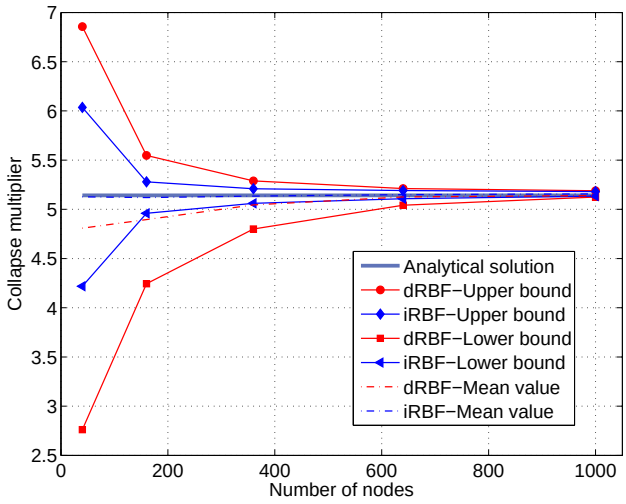

Fig. 3. Bounds on the collapse multiplier versus the number of nodes

In Table 2 the solutions obtained using the present methods with 2560 nodes are compared with those obtained previously by different yield design approaches using FEM, smoothed finite element (SFEM) and EFG simulations. In general, the present solutions are close to results in the literature. Considering upper solutions, the result obtained using the iRBF method is slightly lower than the one obtained using the EFG mesh-free method with the same nodal discretization [12].

5.2 Thin square plates with cutouts subjected to tension load

Next, two thin square plates with a central square cutout and a thin crack subjected to a uniform tension load, as shown in Figure 5, are considered. These problems have been investigated numerically by finite elements [37,39],

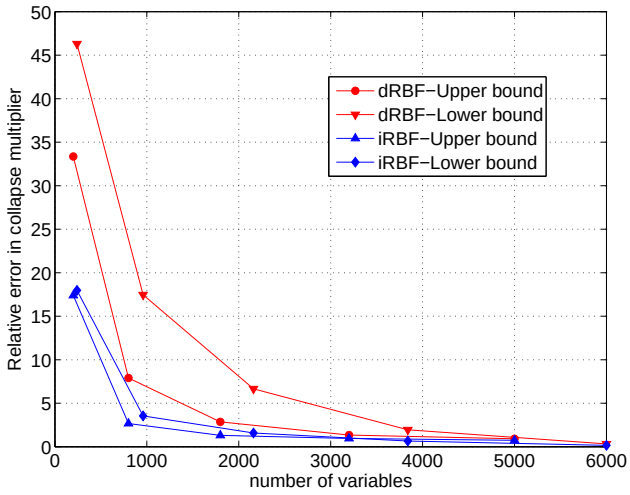

Fig. 4. Relative error in collapse multipliers versus the number of variables

Table 2
The punch of problem: comparison with previous solutions

Authors	Approach	Collapse multiplier	
		Upper-bound	Lower-bound
Present method (dRBF)	Kinematic and static	5.159	5.133
Present method (iRBF)	Kinematic and static	5.146	5.140
Vicente da Silva and Antao [31]	Kinematic	5.264	-
Sloan & Kleeman [32]	Kinematic	5.210	-
Makrodimopoulos et al. [33,34]	Kinematic and static	5.148	5.141
Le et al. [12], EFG	Kinematic	5.147	-
Le et al. [35], SFEM	Kinematic	5.143	-
Capsoni & Corradi [36]	Mixed formulation	5.240	

symmetric Galerkin boundary elements [38], and mesh-free methods [40,41]. Owing to the symmetry, only the top-right quarter of plates is modeled, as shown in Figure 6. Uniform nodal distribution is be used to discretize the computational domain, see Figure 7.

Limit load multipliers obtained using uniform nodal distributions are reported in Tables 3 and 4. Collapse load multiplier versus the number of nodes is also shown in Figure 8. Again, it can be observed that the iRBF-based method can provide more accurate solutions than the dRBF-based method, particularly for the static approach.

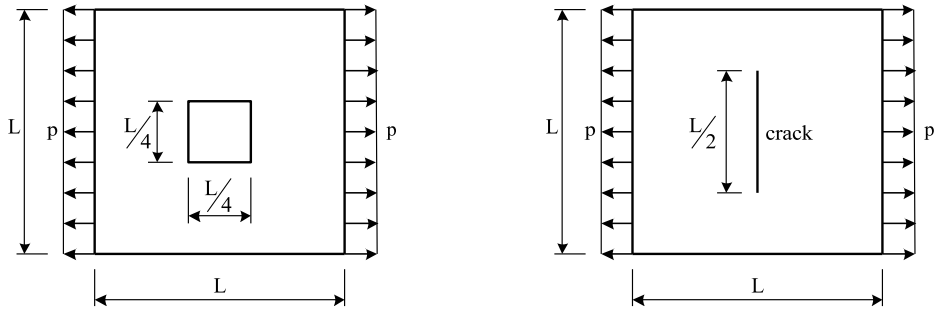

(a) Square cutout (b) Thin crack

Fig. 5. Thin square plates

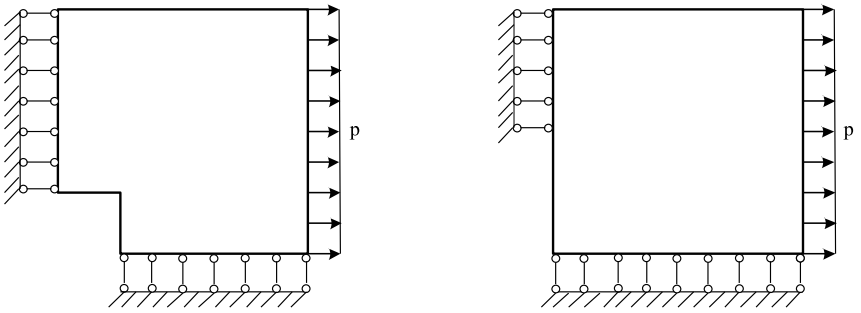

(a) Square cutout (b) Thin crack

Fig. 6. The upper-right quarter of plates

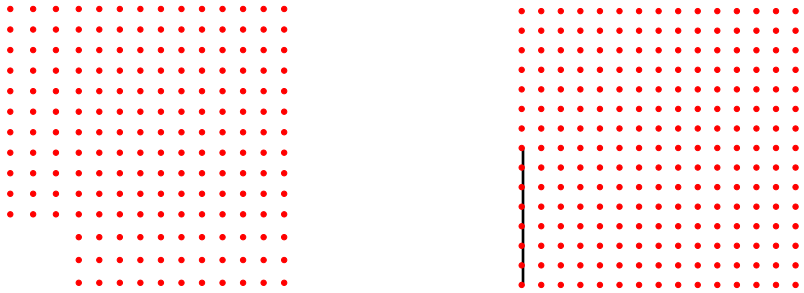

(a) Square cutout (b) Thin crack

Fig. 7. Uniform nodal discretization

Table 3
Collapse multipliers for the square plate with a central square cutout

Nodes	dRBF		iRBF	
	Upper-bound	Lower-bound	Upper-bound	Lower-bound
273	0.750	0.734	0.702	0.712
589	0.750	0.732	0.715	0.726
851	0.749	0.732	0.715	0.729

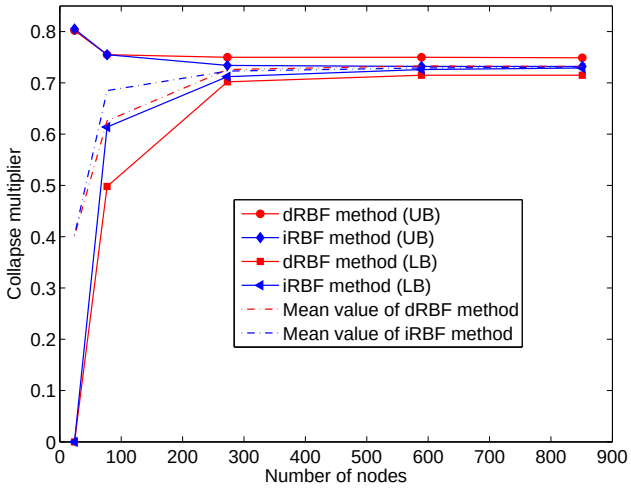

(a) Square cutout

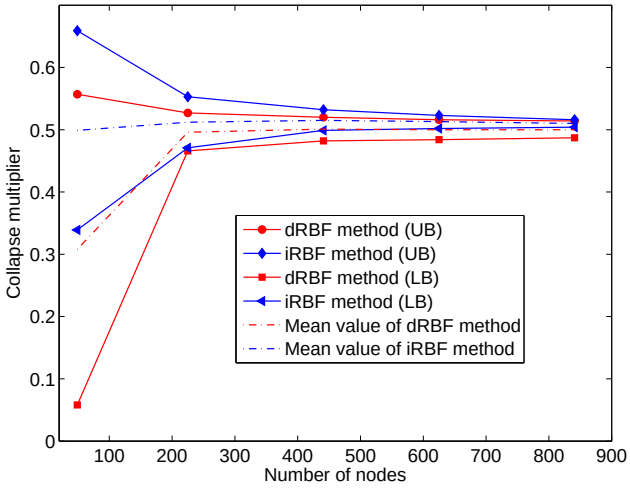

(b) Thin crack

Fig. 8. Convergence of limit load factor for the plates

Table 4
Collapse multipliers for the square plate with a central thin crack

Nodes	dRBF		iRBF	
	Upper-bound	Lower-bound	Upper-bound	Lower-bound
441	0.520	0.482	0.532	0.499
625	0.516	0.484	0.523	0.502
841	0.514	0.487	0.516	0.504

Table 5 shows that the results obtained by using RBF methods are in good agreement with previously reported numerical solutions. Considering upper bound limit factor, the present results are close to Zhou & Liu's solutions, with the maximum error of only 2.79%. It is important to note that the estimated

lower bounds reported in [38,40] are higher than the present lower bound solutions, and surpasses the upper bound of the present iRBF method for the plate with square cutout. This can be explained by the fact that in [38,40] the strong form of the equilibrium equations were transformed into the so-called weak form, and to be satisfied locally in an average sense using approximated virtual displacement fields. Therefore, the static method in [38,40] may result in a higher value than the actual limit multiplier. In contrast, it is clear that all the present lower bound solutions obtained are below the upper bounds reported in Table 5.

Table 5
Plates with cutouts problem: Comparison with previous solutions

Authors	Approach	Square cutout		Thin crack	
		UB	LB	UB	LB
Present method (dRBF)	Kinematic and static	0.749	0.715	0.514	0.487
Present method (iRBF)	Kinematic and static	0.732	0.729	0.516	0.504
Belytschko & Hodge [37]	Static	–	0.693	–	0.498
Zhang et al. [38]	Static	–	0.747	–	0.514
Zhang et al. [39]	Kinematic	0.764	-	0.534	-
Chen et al. [40]	Static	–	0.736	–	0.513
Zhou & Liu (Sibson) [41]	Kinematic	0.753	–	0.515	–
Zhou & Liu (Laplace) [41]	Kinematic	0.752	–	0.513	–

5.3 Notched tensile specimen

Finally, a double notched specimen consists of a rectangular specimen with two thin cracks under in-plane tensile stresses τ_0, as shown in Figure 9, is also considered. This problem exhibits volumetric locking phenomena [42] and became a popular benchmark test for plastic yield design procedures. The locking problem was handled using various techniques proposed in the literature, including higher-order displacement-based finite element method [43], mixed finite elements [36,44,45] and discontinuous elements [46,32,47], mesh-free methods [12], smoothed finite elements [35,48]. Owing the symmetry, only the upper-right quarter of the double notched problem is discretized.

Several uniform nodal distributions are employed. Computed solutions and convergence analysis are presented in Table 6 and Figure 10. Table 7 compares the present solutions with those obtained previously. The mean values of the dRBF and iRBF results are 1.1343 and 1.1342, respectively. It can be

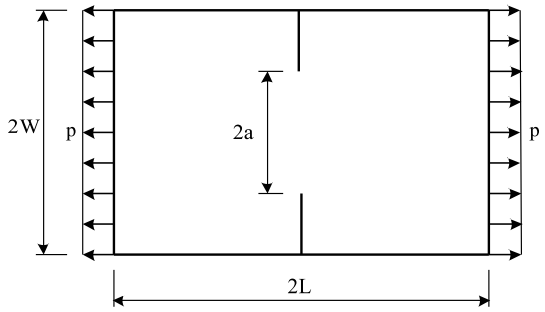

(a) Geometry (W= L = 2a = 1) and loading

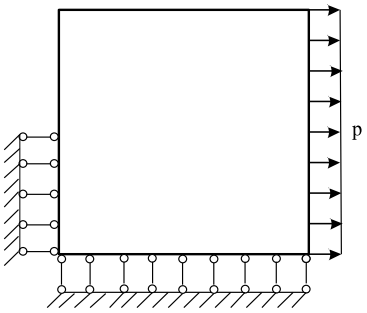

(b) Computational model

Fig. 9. Double notched specimen

observed that these mean values are very close to the benchmark solution obtained using mixed formulation by Christiansen & Andersen [45].

Table 6
Double notched specimen: limit load multiplier

Nodes	dRBF				iRBF			
	Upper-bound		Lower-bound		Upper-bound		Lower-bound	
	λ^+	e(%)	λ^-	e(%)	λ^+	e(%)	λ^-	e(%)
289	1.156	0.21	1.092	5.56	1.150	0.56	1.100	2.79
441	1.152	0.33	1.116	2.24	1.146	0.34	1.114	1.31
625	1.149	0.29	1.120	0.37	1.143	0.23	1.122	0.66
841	1.146	0.20	1.122	0.20	1.141	0.15	1.127	0.48

6 CONCLUSIONS

The present contribution has presented displacement and equilibrium meshfree formulation based on integrated radial basis functions (iRBF) for dual yield design problems. In the kinematic formulation, the high-order approximation of the displacement fields using the integrated radial basis functions

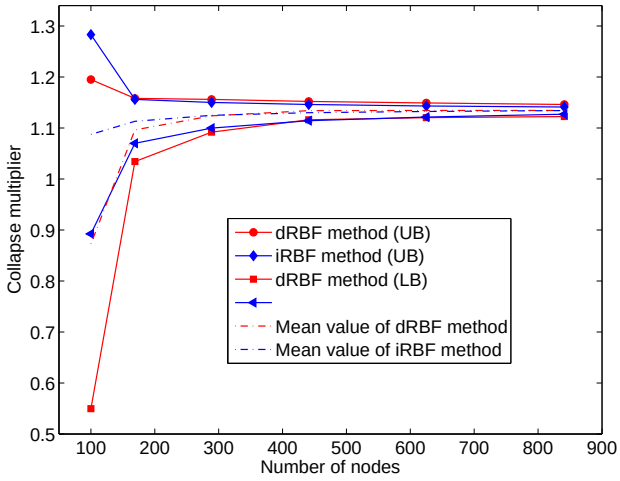

Fig. 10. Convergence study for the double notched specimen problem

Table 7
The double notched specimen: comparison with previous solutions

Authors	Approach	Collapse multiplier	
		Upper-bound	Lower-bound
Present method (dRBF)	Kinematic and static	1.146	1.122
Present method (iRBF)	Kinematic and static	1.141	1.127
Ciria et al. (Uniform) [49]	Kinematic and static	1.149	1.131
Ciria et al. (Adaptive) [49]	Kinematic and static	1.139	1.132
Le et al. [35]	Kinematic	1.137	-
Le et al. [12]	Kinematic	1.154	-
Krabbenhoft et al. [50]	Static	-	1.132
Tin-Loi & Ngo [43]	Static	-	1.166
Christiansen et al. [45]	Mixed formulation	1.136	

can prevent volumetric locking. Moreover, direct nodal integration of the iRBF approximation not only results in inexpensive computational cost, but also overcomes the instability problems. In the static formulation, with the use of iRBF approximation of the stress fields in combination with the collocation method, equilibrium equations and yield conditions only need to be enforced at the nodes, leading to the reduction in computational effort. It has been shown in several examples that the mean values of the iRBF upper and lower bounds are accurate, and can be considered as the actual collapse load multiplier for most practical engineering problems, for which exact solution is unknown.

Acknowledgements

This research has been supported by the Institute for Computational Science and Technology (ICST), Ho Chi Minh City.

References

1. M.A. Save, C.E. Massonnet, G. de Saxce. Plastic Analysis and Design of Plates, Shells and Disks. North-Holland Series in Applied Mathematics and Mechanics, vol. 43. Elsevier: Amsterdam, 1997.

2. J. Salencon. Yield Design. Wiley. com, 2013.

3. S.W. Sloan. Lower bound limit analysis using finite elements and linear programming. *International Journal for Numerical and Analytical Methods in Geomechanics*, 12:61-77, 1988.

4. S. Krenk, L. Damkilde, O. Hoyer. Limit analysis and optimal design of plates with equilibrium elements. *Journal of Engineering Mechanics*, 120:12371254, 1994.

5. P.N. Poulsen, L. Damkilde. Limit state analysis of reinforced concrete plates subjected to in-plane forces. *International Journal of Solids and Structures*, 37:6011-6029, 2000.

6. K. Krabbenhoft, L. Damkilde. Lower bound limit analysis of slabs with nonlinear yield criteria. *Computers and Structures*, 80:2043-2057, 2002.

7. T. Belytschko and Y.Y. Lu and L. Gu. Element-free Galerkin methods. *International Journal for Numerical Methods in Engineering*, 37:229256, 1994.

8. S. S. Chen, Y. H. Liu and Z. Z. Cen. Lower-bound limit analysis by using the EFG method and non-linear programming *International Journal for Numerical Methods in Engineering*, 74:391–415, 2008.

9. C.V. Le, H. Askes, M. Gilbert. Adaptive Element-Free Galerkin method applied to the limit analysis of plates *Computer Methods in Applied Mechanics and Engineering*, 199:2487–2496, 2010.

10. C.V. Le, M. Gilbert, H. Askes. Limit analysis of plates using EFG method and second order cone programming. *International Journal for Numerical Methods in Engineering*, **78**:1532–1552, 2009.

11. C.V. Le, M. Gilbert and H. Askes. Limit analysis of plates and slabs using a meshless equilibrium formulation. *International Journal for Numerical Methods in Engineering* 83:1739–1758, 2010.

12. C.V. Le, H. Askes and M. Gilbert. A locking-free stabilized kinematic EFG model for plane strain limit analysis *Computers and Structures*, 106-107: 1–8, 2012.

13. R. Franke. Scattered data interpolation: tests of some methods. *Mathematics of Computation*, 38:181, 1982.

14. R. Franke and R. Schaback. Solving partial differential equations by collocation using radial functions. *Applied Mathematics and Computation*, 93:73–82, 1998.

15. G.E. Fasshauer. Solving differential equations with radial basis functions: multilevel methods and smoothing. *Advances in Computational Mathematics*, 11:139–159, 1999.

16. N. Mai-Duy and T. Tran-Cong. Numerical solution of differential equations using multiquadric radial basis function networks. *Neural Networks*, 14 (2), 185–199, 2001.

17. A.H.D. Cheng, M.A. Golberg, E.J. Kansa and G. Zammito. Exponential convergence and H–c multiquadrics collocation method for partial differential equations. *Numer. Methods Partial Differential Equations*, 19:571–594, 2003.

18. H.Y. Hu and Z.C. Li and A.H.D. Cheng. Radial basis collocation method for elliptic equations. *Computers and Mathematics with Application*, 50:289–320, 2005.

19. H.Y. Hu and J.S. Chen and W. Hu. Weighted radial basis collocation method for boundary value problems. *International Journal for Numerical Methods in Engineering*, 69:2736–2757, 2007.

20. G.R. Liu and Y.T. Gu. A local radial point interpolation method (LRPIM) for free vibration analyses of 2-D solids. *Journal of Sound and Vibration*, 246(1):29–46, 2001.

21. J.R. Xiao and M.A. McCarthy. A local Heaviside weighted meshless method for two-dimensional solids using radial basis functions. *Computational Mechanics*, 31:301–315, 2003.

22. G.R. Liu, G.Y. Zhang, Y.T. Gu and Y.Y. Wang. A meshfree radial point interpolation method (RPIM) for three-dimensional solids. *Computational Mechanics*, 36:421430, 2005.

23. J.S. Chen, L. Wang, H.Y. Hu and S.W. Chi. Subdomain radial basis collocation method for heterogeneous media. *International Journal for Numerical Methods in Engineering*, 80:163–190, 2009.

24. P. Xia, S.Y. Long, H.X. Cui and G.Y. Li. The static and free vibration analysis of a nonhomogeneous moderately thick plate using the meshless local radial point interpolation method. *Engineering Analysis with Boundary Elements*, 33:770–777, 2009.

25. L. Wang, J.S. Chen and H.Y. Hu. Subdomain radial basis collocation method for fracture mechanics. *International Journal for Numerical Methods in Engineering*, 83:851–876, 2010.

26. A. Khosravifard and M.R. Hematiyan and L. Marin. Nonlinear transient heat conduction analysis of functionally graded materials in the presence of heat sources using an improved meshless radial point interpolation method. *Applied Mathematical Modelling*, 35:4157–4174, 2011.

27. E. Christiansen. Limit analysis of collapse states. *Handbook of numerical analysis, vol. IV, Amsterdam: North-Holland*, 1996. p. 193312 [chapter II].

28. N. Mai-Duy and T. Tran-Cong. Approximation of function and its derivatives using radial basis function networks. *Applied Mathematical Modelling*, 27:197–220, 2003.

29. N. Mai-Duy and T. Tran-Cong. An Efficient Indirect RBFN-Based Method for numerical solution of PDEs. *Numerical Methods for Partial Differential Equations*, 21:770–790, 2005.

30. L. Prandtl. Ueber die Haerte plastischer Koerper. *Nachrichtex der Akademie der Wissenschaften in Gottingen. II. Mathematisch-Physikalische Klasse II*, 12:74–85, 1920.

31. M. Vicente da Silva and A.N. Antao. A non-linear programming method approach for upper bound limit analysis. *International Journal for Numerical Methods in Engineering*, 72:1192–1218, 2007.

32. S.W. Sloan and P.W. Kleeman. Upper bound limit analysis using discontinuous velocity fields. *Computer Methods in Applied Mechanics and Engineering*, 127:293–314, 1995.

33. A. Makrodimopoulos and C.M. Martin. Upper bound limit analysis using simplex strain elements and second-order cone programming. *International Journal for Numerical and Analytical Methods in Geomechanics*, 31:835–865, 2006.

34. A. Makrodimopoulos and C.M. Martin. Lower bound limit analysis of cohesive-frictional materials using second-order cone programming. *International Journal for Numerical Methods in Engineering*, 66:604–634, 2006.

35. C.V. Le, H. Nguyen-Xuan, H. Askes, S. Bordas, T. Rabczuk, and H. Nguyen-Vinh. A cell-based smoothed finite element method for kinematic limit analysis. *International Journal for Numerical Methods in Engineering*, 83:1651–1674, 2010.

36. A. Capsoni and L. Corradi. A finite element formulation of the rigid-plastic limit analysis problem. *International Journal for Numerical Methods in Engineering*, 40:2063–2086, 1997.

37. T. Belytschko and P.G. Hodge. Plane stress limit analysis by finite element. *Journal of the Engineering Mechanics Division*, 96:931–944, 1970.

38. X.F. Zhang, Y.H. Liu, Y.N. Zhao and Z.Z. Cen. Lower bound limit analysis by the symmetric Galerkin boundary element method and the complex method. *Computer Methods in Applied Mechanics and Engineering*, 191:1967–1982, 2002.

39. F. Zhang, L. Mingwan and H. Kehchih. A mathematical programming algorithm for limit analysis. *Acta Mechanica Sinica*, 7:267–274, 1991.

40. S. Chen, Y. Liu, Z. Cen. Lower-bound limit analysis by using the EFG method and non-linear programming. *International Journal for Numerical Methods in Engineering*, 74:391–415, 2008.

41. S.T. Zhou and Y.H. Liu. Upper-bound limit analysis based on the natural element method. *Acta Mechanica Sinica*, 28:1398–1415, 2012.

42. J.C. Nagtegaal, D.M. Parks and J.C. Rice. On numerically accurate finite element solutions in the fully plastic range. *Computer Methods in Applied Mechanics and Engineering*, 4:153–177, 1974.

43. F. Tin-Loi and N.S. Ngo. Performance of the p-version finite element method for limit analysis. *International Journal of Mechanical Sciences*, 45:1149–66, 2003.

44. K.D. Andersen, E. Christiansen and M.L. Overton. Computing limit loads by minimizing a sum of norms. *SIAM Journal on Scientific Computing*, 19:1046–62, 1998.

45. E. Christiansen and K.D. Andersen. Computation of collapse states with von Mises type yield condition. *International Journal for Numerical Methods in Engineering*, 46:1185–1202, 1999.

46. A. Bottero, R. Negre, J. Pastor and S. Turgeman. Finite element method and limit analysis theory for soil mechanics problems. *Computer Methods in Applied Mechanics and Engineering*, 22:131–49, 1980.

47. A.V. Lyamin and S.W. Sloan. Upper bound limit analysis using linear finite elements and nonlinear programming. *International Journal for Numerical and Analytical Methods in Geomechanics*, 26:181–216, 2002.

48. C. V. Le, H. Nguyen-Xuan, H. Askes, T. Rabczuk, and T. Nguyen-Thoi. Computation of limit load using edge-based smoothed finite element method and second-order cone programming. *International Journal of Computational Methods*, 10:1340004, 2013.

49. H. Ciria, J. Peraire and J. Bonet. Mesh adaptive computation of upper and lower bounds in limit analysis. *International Journal for Numerical Methods in Engineering*, 75:899–944, 2008.

50. K. Krabbenhoft and L. Damkilde. A general nonlinear optimization algorithm for lower bound limit analysis. *International Journal for Numerical Methods in Engineering*, 56:165–184, 2003.

51. C.V. Le, H. Nguyen-Xuan, H. Nguyen-Dang. Upper and lower bound limit analysis of plates using FEM and second-order cone programming. *Computers and Structures*, 88:65–73, 2010.

52. D. T. Tran, C.V. Le. Extended finite element method for plastic limit load computation of cracked structures. *International Journal for Numerical Methods in Engineering*, 104:2–17, 2015.

53. C.V. Le, P.H. Nguyen, T.Q. Chu. A curvature smoothing Hsieh-Clough-Tocher element for yield design of reinforced concrete slabs. *Computers and Structures*, 152:59–65, 2015.

54. C.V. Le, P.L.H. Ho, P.H. Nguyen, T.Q. Chu. Yield design of reinforced concrete slabs using a rotation-free meshfree method. *Engineering Analysis with Boundary Elements*, 50:231–238, 2015.